Journal of the Korean Society for Nondestructive Testing
Vol. 22, No. 6 (2002. 12)

Characterisation of Tensile Deformation through Infrared Imaging Technique

B. Venkataraman, Baldev Raj† and C. K. Mukhophadyay

Abstract It is well known that during tensile testing, a part of the mechanical work done on the specimen is transformed into heat energy. However, the ultimate temperature rise and the rate of temperature rise is related to the nature of the material, conditions of the test and also to the deformation behaviour of the material during loading. The recent advances in infrared sensors and image / data processing techniques enable observation and quantitative analysis of the heat energy dissipated during such tensile tests. In this study, infrared imaging technique has been used to characterise the tensile deformation in AISI type 316 nuclear grade stainless steel. Apart from identifying the different stages during tensile deformation, the technique provided an accurate full-field temperature image by which the point and time of strain localization could be identified. The technique makes it possible to visualise the region of deformation and failure and also predict the exact region of fracture in advance. The effect of thermal gradients on plastic flow in the case of interrupted straining revealed that the interruption of strain and restraining at a lower strain rate not only delays the growth of the temperature gradient, but the temperature rise per unit strain decreases. The technique is a potential NDE tool that can be used for on-line detection of thermal gradients developed during extrusion and metal forming process which can be used for ensuring uniform distribution of plastic strain.

Keywords: Infrared imaging, tensile deformation, stress, strain, strain rate, temperature

1. Introduction

Surface temperature measurements are useful for many industrial applications and materials characterisation. Such measurements can be made with contact or non-contact. Contact methods include use of thermometers or thermocouples. While contact methods find widespread applications, the inherent disadvantages include (a) point measurements (b) for measurement of large areas a large number of such devices need to be attached and the temperatures at points between these devices must be estimated by interpolation, (c) perfect contact needs to be ensured between the measurement surface and the temperature probe. In field conditions, there is always the risk of the probe getting detached by thermal or mechanical stress or may get damaged due to harsh environmental conditions. Further, contact techniques may distort the temperature distribution being measured.

An attractive and alternative method for surface temperature measurement is the non contact method through the measurement of infrared radiation emitted by the object. It is well known that any body above absolute zero emits electro-magnetic radiation. At ambient temperatures, these radiation are predominantly in the infrared band of the electromagnetic spectrum. The energy and intensity

Received September 9, 2002. † Corresponding author: Materials, Chemical and Reprocessing Group, Indira Gandhi Centre for Atomic Research, Kalpakkam - 603 102, India E-mail: dmg@igcar.ernet.in

of infrared radiation emitted by the object depends on its temperature, surface condition and viewing angle and can be calculated using the Weins law, Plancks law and Stefan Boltzmann law. It is possible to convert these IR radiation into electrical signals which can then be displayed on a monitor as a grey level image or colour image in which different grey levels or colours represent different temperatures. Thus, a complete surface temperature map of the object can be obtained in a non contact way. With appropriate calibration, it is also possible to get the absolute temperature values of any point on the surface of the object. This nondestructive technique also referred to as infrared imaging or thermal imaging or thermography finds extensive applications for detection of hot spots and condition monitoring in electrical (Venkatraman et al. 1992), petrochemical (Raj et al. 1992) and steel industries (Rogers 1978), determination of mould temperatures for process control (Maldague, 1993), laser heat treatment (Rockstroh Mazumdar, 1985), thermal management of electronic modules (Hoffer et al. 1986), impact testing of polymer foams (Roberts 1983), weld monitoring (Chin et al. 1983; Venkatraman. et al. 1993; Raj et al. 1998), and a variety of other applications.

It is well known that during tensile testing, a part of the mechanical work done on the specimen is transformed into heat energy. However, the ultimate temperature rise and the rate of temperature rise is related to nature of the material, conditions of the test and also to the deformation behaviour of the material during loading. Thus by using infrared imaging, it is possible to detect the variations in temperature and consequently predict the deformation behavior of the material. Limited experimental work has been reported in literature. Wilburn (1977) used two infrared radiometers to observe the profiles of temperature distribution during tensile testing of SAE 4130 steel. Huang (1980), used an infrared sensor of JWH-3 type to study the temperature profiles developed during tensile testing of low carbon steel, medium carbon steel and stainless steel. However, in both these cases, the infrared sensors had low spatial and temporal resolutions. They averaged the temperature from a large projected area on the centre of the tensile bar. With the rapid advances in electronics and instrumentation, focal plane arrays with temperature resolutions of the order of 0.1K or better and spatial resolutions of the order of about 100-200 microns are available. At the authors' lab, a systematic study has been made on the use of infrared imaging as an NDE tool for characterisation of the tensile deformation of nuclear grade austenitic stainless steel (Venkataraman et al. 2000).

The purpose of this paper is to highlight that recent advances in infrared sensors and image / data processing techniques enable observation and quantitative analysis of the dissipative effects that accompany tensile deformation. Localisation due to necking can also be observed by this technique. The effect of interrupted straining on the development of thermal gradients is also described.

2. Experimental Setup and Procedure

Flat tensile specimens with guage dimensions of 50mm x 200mm x 3 mm were prepared from solution annealed (1323 K/1h/Water Quench) of nuclear grade AISI type 316 stainless plates steel(SS). The chemical composition of this steel is

Table 1 Chemical composition (wt%) of AISI type 316 stainless steel

Element	C	Cr	Ni	Mn	Mo	P	S	Si	Va
Composition (wt. %)	0.035	17	10.9	1.5	2	0.035	<0.003	0.6	0.08

Element	Co	Cu	As	Pb	Al	Nb	Sn	Ti	W
Composition (wt. %)	0.19	0.25	< 0.006	< 0.006	< 0.034	< 0.07	< 0.004	< 0.08	<0.1

given in Table 1.

More than 50 specimens were prepared. All the specimens were polished with a 400 grit emery paper to obtain a uniform surface finish. Metallography carried out on the samples indicated a typical grain size of the order of 50 μm. Very few inclusions were observed and the size of the inclusions was less than 2 μm. In order to ensure that no volumetric defects were present, the specimens were subjected to radiography. The radiographic sensitivity was 1.6 % of the thickness.

Tensile testing was carried out using INSTRON 1195 tensile testing machine at five different strain rates representing a broad range spanning from a slow strain rate of 3.3 x 10^{-4} s^{-1} to a comparatively fast strain rate of 1.7 x 10^{-2} s^{-1}. Fig. 1 shows a schematic of the experimental setup.

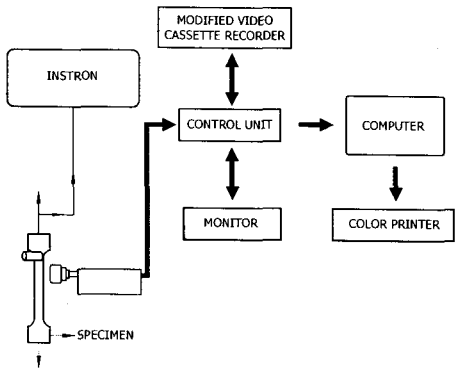

Fig. 1 Schematic of the experimental setup for tensile deformation studies

Thermal images of the specimens during tensile deformation were captured using an Agema Thermovision - 550. This is a based on a focal plane array with a spectral sensitivity in the range of 3 - 5.6 micrometers. It has a built-in 20° lens. The IR camera measures and images the emitted infrared radiation from an object. The fact that radiation is a function of object surface temperature makes it possible for the camera to calculate and display this temperature. The image is high resolution colour image appearing in real-time either in the integral viewfinder or on an external monitor. It is possible to capture and store images onto a removable PC-Card. The images can be analysed either in the field by using the real-time measurement functions built into the camera, or in a PC by using the IR Win 5.0 reporting and analysis software. The IR camera was mounted on to a tripod and located at a distance of 0.5m from the specimen. The camera was focused on to the specimen.

Since small temperature variations were to be measured, adequate precautions had to be taken. To overcome the effects of emissivity, a thin coat of black paint was applied to the gage length of the specimen. The entire experimental setup was arranged at a place far from ventilation ducts. This ensured that sudden air drafts do not occur which can alter the temperature. The ambient temperature was 299 K and the relative humidity 60 %. Both of these were maintained constant during the period of experiment.

3. Results and Analysis

Tensile properties of AISI type 316 stainless steel are shown in Table 2. The results indicate the average of at least three measurements for each strain rate. A slight increase in ultimate strength and reduction in ductility are observed with increasing strain rate. Yield strength values do not show a clear trend of increase or decrease.

Table 2 Tensile test results

Strain Rate (s^{-1})	0.2 % offset Yield Strength (MPa)	Ultimate Tensile Strength (UTS) (MPa)	Total Elongation (%)	Uniform Elongation %
3.3 x 10^{-4}	209	528	78	70
6.7 x 10^{-4}	222	556	72	65
1.7 x 10^{-3}	219	558	68	61
3.3 x 10^{-3}	253	568	61	51
6.7 x 10^{-3}	258	578	57	47
1.7 x 10^{-2}	268	578	56	45

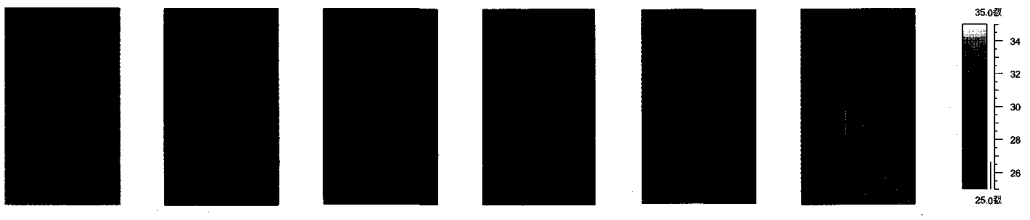

2.4% (a) 15.4% (b) 34.2% (c) 47% (d) 70.5% (e) 74.2% (f)

Fig. 2 Thermal Images for typical nominal strain at rate of 3.3 X 10^{-4} s^{-1}

7.4% (a) 15.2% (b) 24.4% (c) 47.2% (d) 59.7% (e) 66.2% (f)

Fig. 3 Thermal Images for typical nominal strain at rate of 6.7 X 10^{-4} s^{-1}

7.1% (a) 26.5% (b) 47.3% (c) 54.2% (d) 58.9% (e) 60% (f)

Fig. 4 Thermal Images for typical nominal strain at rate of 1.7 X 10^{-3} s^{-1}

The different manifestations accompanying the plastic deformation of AISI type 316 SS are presented in Figs. 2(a) - (f), 3 (a-f) and 4(a-f). They give an overview of the thermal dissipation as a function of strain and strain rate. The progressive rise in temperature with increasing strain levels and strain rates can be clearly visualized from the thermal patterns.

3.1. Variation of Temperature with Nominal Strain

To simplify data interpretation and for quick visualisation of the phenomenon, a graphical plot of temperature versus strain for a strain rate of 6.7 x 10^{-3} s^{-1} is presented in Fig. 5. The stress vs strain for the same strain rate is superimposed on this. The curve in general can be divided into three distinct regions.

Region I - start of the test to just before yield point.

Region II - from yield point to UTS and

Region III - from UTS to fracture.

Region I in case of low strain rates indicates a initial rise followed by a small dip in the tempera- ture. This drop in temperature is very small of the order of 0.2 K - 0.4 K. Region II is characterized by rise in temperature. This rise with strain is quite gradual as is evident from the graph. In the Region III, there is a significant rise in temperature with strain which reaches a maximum at fracture.

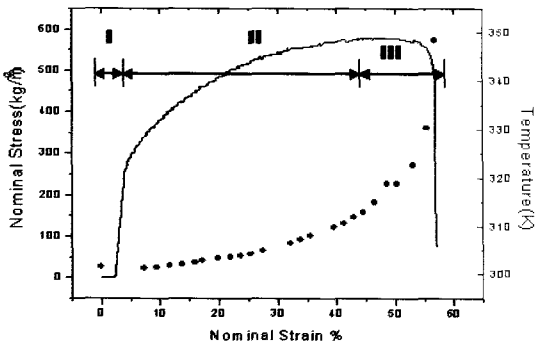

Fig. 5 Plot of stress, strain and temperature for a strain rate of 6.7 x 10^{-3} / s

The slight drop in the temperature in the elastic region is attributed to the thermoelastic effect (Caglioti, 1986). It is well known that there exists an interrelationship between the stress and strain (mechanical work done on a material) in the elastic range and changes in its thermodynamic properties i.e. the temperature and entropy. When an elastic stress is applied rapidly to a tensile specimen such that the maximum stress is reached before the specimen can exchange any thermal energy with the surroundings, the heat transferred to or from the specimen is negligible. So the change in internal energy is caused only by the mechanical work done on the material and the stressing is isentropic i.e. occurring at constant entropy and is reversible. For uniaxial adiabatic straining, the change in the temperature of the specimen with strain is given by (Dieter, 1988)

$$\delta T/\delta \varepsilon = -V_m \alpha E T/ C_v \qquad \cdots\cdots (1)$$

where, $\delta T/\delta \varepsilon$ represents the change in temperature with strain at constant entropy, Vm is the molar volume of the specimen, α is the linear thermal expansion coefficient of the specimen, E is the isothermal Young's modulus, T is the temperature in Kelvin, C_v is the specific heat at constant volume. Practically all the materials exhibit a volume expansion on heating. Since α is positive and V, T, E and C_v are also positive, adiabatic elastic tension lowers the temperature of the material. It has been mentioned that this temperature change would be very small of the order of about 0.2 K (Caglioti, 1986). In our experiments, this temperature drop has been observed to vary in the range of about 0.2K - 0.4K.

The initial drop is followed by a sudden increase in temperature as plastic deformation begins. This inversion of temperature indicates the transition between the elastic and plastic behaviour of the material (Bordoni, 1986). With increasing strain levels, the temperature continues to increase. Region II is the work hardening region characterised by a rise in temperature till UTS point. This rise in temperature during plastic flow can be explained as follows :

The energy relationship during plastic flow is given by

$$E_m = E_e + E_w \qquad \cdots\cdots (2)$$

Where, E_m is the mechanical work done, E_e is the energy expended in elastic deformation and is recoverable, E_w is the energy expended in plastic deformation and

$$E_w = E_s + E_h \qquad \cdots\cdots (3)$$

Where, E_s is the energy stored as the strain energy of dislocations and E_h is the energy dissipated as heat. By classical thermodynamic treatment of the deformation process, only the thermal energy release has been considered in eqns. (2) and (3). However, if we consider other forms of energy release, then we can combine eqns. (2) and (3) and rewrite as

$$E_m = E_e + E_s + E_h + E_{AE} + E_{exo\text{-}e} + \ldots\ldots \qquad \cdots\cdots (4)$$

where E_{AE} is the energy released in the form of acoustic waves and $E_{exo\text{-}e}$ is the exo-emission which relates to the emission of negatively charged particles from the material surface during excitation by plastic deformation (Misra, 1975). Baldev Raj (Raj, 1986) had indicated that AE signals with a wide range of amplitudes are likely to be generated during plastic deformation. However, considering the dynamics of dislocation and the detection threshold based on the transducer wave sensitivity

(10^{-13}m), source to transducer distance (0.1m) etc, it was deduced that such signals would be very weak and below the detectable thresholds except at the yield region where dislocation multiplications give strong AE signals (Raj, 1986). Hence eqn. (4) can be approximated as

$$E_m = E_e + E_s + E_h \quad \cdots\cdots (5)$$

Work done during plastic deformation is a thermodynamically irreversible process. As observed from eqn. (5) above, a major portion of the total mechanical work done during plastic flow is dissipated as heat which raises the temperature of the material while being deformed. A small but significant percentage, however, is stored in the metal in the form of lattice defects, mainly dislocations. It has been observed that the amount of heat evolved as a percentage of plastic work expended in the tensile deformation is about 86.5% for steel, 90.5-92% for copper, 92-93% for polycrystalline aluminium and 95-95.5% for aluminium single crystal (Gao and Wagoner, 1987). Heat generated at each point of the specimen is proportional to the energy dissipated (E_h) by the specimen at each point and thus proportional to the level of stress at the point. As the specimen is deformed plastically, work hardening takes place. That is, the stress required to cause additional strain in this region increases with plastic strain. As a result, the heat generated at each point increases with plastic strain. The main mechanism of heat loss during tensile deformation can be considered to be due to conduc- tion. Convection losses can be considered to be negligible due to small temperature difference between the surrounding and the specimen. Thus, with increasing strain levels, the rate of generation of heat exceeds the rate of conduction. This produces a perceptible rise in the temperature of the specimen.

In general, strain hardening increases the specimen load carrying capacity. However, at UTS the effect of strain hardening is overcome by the reduction in cross-sectional area of the specimen, resulting in the decrease in its load carrying capacity. Consequently, localized deformation results. This condition is seen as necking of the tensile specimen. As is evident from Fig. 5, the necking of the specimen manifests as a maximum in the engineering stress-strain curve. A large rise in temperature is observed which results in the change in the slope of the strain vs. temperature curve.

An interesting observation is that the formation of neck results in peeling of the coating applied in the gauge region. It is to be mentioned here that a very thin coat was applied to take care of emissivity variations of the specimen. During the process of necking, substantial temperature rise occurs especially at higher strain rates (more than 25 K above ambient at 10^{-2} s^{-1}) which results in the peeling off of the thin coating in the vicinity of necking region.

The results obtained by us are different from those presented by Huang et. al. in which they had indicated no temperature rise till yielding and also a initial flat region in the work hardening phase. The infrared system used by them averaged the temperature from a comparatively large projected area of 25 mm x 5 mm. Since the rise in temperature in the elastic region and initial phase of work hardening is small, this could have been missed due to the lower sensitivity and spatial resolution of the infrared system used.

3.2. Effect of Strain Rate on Thermal Emission

Fig. 6 is a graphical plot of the variation of nominal strain with maximum temperature along gage length of the specimens for different strain rates. It can be observed that all the graphs exhibit a similar trend of increasing temperature with increasing strain level. The temperatures were profiled along the gage length of the specimen. Table 3 gives the maximum temperature observed in the gage region for nominal strains of 7.3 %, 15.4%, 27%, 34.2%, 47.7% and 56.5% as a function of strain rate. It is observed from Table 3 that at low strain levels and intermediate strain rates, a clear trend in temperature is not apparent. This can be

Table 3 Variation of temperature along gage length for different strains and strain rates

Nominal Strain % ↓ / Strain rate →	Temperature in gage length (K)					
	3.3×10^{-4}	6.7×10^{-4}	1.7×10^{-3}	3.3×10^{-3}	6.7×10^{-3}	1.7×10^{-2}
7.3	299.9	302.5	300.3	302.7	301.3	303.9
15.4	300.1	302.6	301.9	303	302.4	304.3
27	300.2	302.9	302.4	304.6	304.9	308.6
34.2	300.8	303.1	304.6	306.5	307.2	309.4
47.7	301.4	304.0	306.7	310.8	314.9	320.0
56.5	301.7	304.5	310.0	320.7	334.8	360.1

attributed to the fact that at low strain levels upto around 20 % nominal strain, the temperature rise is not appreciable as can be observed from Fig. 6. Further, for the sake of uniformity in comparison, the temperature values at intermediate nominal strain have been obtained by interpolation of the data. This could also be a cause for this fluctuating trend. However, at nominal strain of 27 % and higher, a clear trend of increasing temperature with increasing strain rate can be observed.

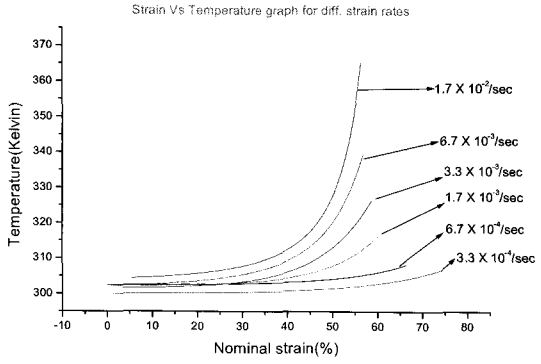

Fig. 6 Plot of nominal strain Vs temperature as a function of Strain rate

The rise in temperature of the specimen with the strain rate for the same values of strain can be explained as follows. As the specimen is deformed plastically, work hardening takes place. It is well known that plastic deformation is due to the motion of a large number of dislocations. The rate of plastic deformation that is the strain rate $\dot{\varepsilon}$ is proportional to the Boltzmann's probability factor:

$$\dot{\varepsilon} \propto \exp\ (-Q/kt) \qquad \cdots\cdots (6)$$

where Q is the activation energy for dislocation motion. Q arises from the activation barrier that a dislocation faces in moving from one minimum energy position to next. The above equation indicates that a dislocation can change its position solely due to thermal fluctuations even without the application of an external stress. Such motion would be random in nature where a dislocation would have an equal probability of moving to the next minimum energy position in any direction. Such motions however would not result in plastic deformation. A certain threshold stress is thus necessary for dislocations to move in a specified direction. If τ_{PN} is the stress required to move a dislocation in the absence of thermal energy (at 0 K) and τ_{app} is the applied stress at 0 K then

$$Q = (\tau_{pn} - \tau_{app})\gamma \qquad \cdots\cdots (7)$$

where γ is the activation volume. Substituting this in eqn. (6) we have

$$\dot{\varepsilon} \propto \exp\left(\frac{[\tau_{pn} - \tau_{app}]}{KT}\ \gamma\right) \qquad \cdots\cdots (8)$$

For a given material γ and τ_{PN} are constant. It can thus be observed from this equation that when a experiment is performed at constant ambient temperature (299 K in the present case), the strain rate is proportional to the applied stress. Higher the strain rate, higher would be the stress. The heat generated at each point on the specimen is proportional to the energy dissipated by the specimen at that point and thus proportional to the

level of stress at the point. Hence for the same nominal strain, higher strain rate produces a higher energy thus resulting in the higher temperature.

An additional cause responsible for this rise in temperature is the mechanism of energy dissipation. At lower strain rates, heat is generated rather slowly by the deformation process and is dissipated to the surroundings quickly resulting in lower rise in the temperature. But with increasing strain rate, the deformation process tends towards an adiabatic one, i.e., the rate at which the heat is generated is much higher compared to the rate at which heat is dissipated from the specimen causing the temperature to rise to a higher value as compared to the temperature attained for the same strain levels at a lower strain rate.

3.3. Thermal Images Predict the Zone of Failure

Fig. 7 shows a typical plot of the variation of temperature on the specimen along its gage length as a function of nominal strain and for a strain rate 6.7×10^{-3} s^{-1}. The point of maximum temperature was determined through thermal profiling for each nominal strain and the graph has been plotted for temperatures on either side of the maximum point on the specimen. The data in Fig. 7 has been fitted using the Lorentz equation

$$Y = Y_0 + \frac{2A}{\pi} \frac{W}{4(\chi - \chi_c) + W^2} \quad \ldots\ldots (9)$$

The results can be correlated with the mechanism of fracture in ductile metals. There are three stages (Vanstone et.al, 1985) by which a ductile material may fail during tensile test. These are nucleation of internal cavities during plastic flow, growth of the cavities with deformation and coalescence of cavities to produce complete rupture. But the onset and progress of these stages may vary depending on materials and the state of stress existing during deformation. The cavities are nucleated heterogeneously at sites where compatibility of deformation is difficult and the preferred sites are inclusions, precipitates, dispersoids etc. These cavities can be

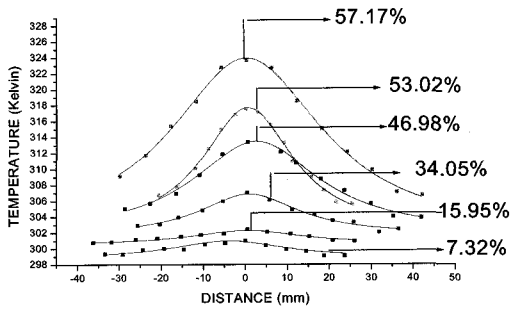

Fig. 7 Temperature profile along gauge length for different strain levels for a strain rate of 6.7 x 10^{-3}/sec

dispersed throughout the gauge length. Thus, it can be observed from Fig. 7 that at low strain levels of the order of 10% - 15% in the work hardening region, the temperature rise along the gauge length is almost uniform.

With the progressive increase in strain, the voids tend to grow. Void growth is the process of cavity enlargement by highly localized plastic deformation. There are at least two distinct mechanisms of void growth. In one, the cavity growth is controlled by plastic flow of matrix material that surrounds the void nucleating phase. Voids of this type (Argon et. al, 1975) tend to grow in a manner that preserves a spherical or ellipsoidal shape in order to minimize surface and local plastic energies. In the second case, the first type of void growth is assisted by decohesion at smaller second phase particles during the deformation process. Void growth is a function of strain and strain rate, increases with void size and varies exponentially with triaxial tension (Raj, 1986). Thus during this stage, the temperature rises along the gauge length, but tends to have a peak in the region of plastic deformation where strain tends to localize. In general, as can be observed from Fig. 7, at about 34 % strain level, the zone at which the failure is likely to occur becomes quite marked with temperature being the precursor to indicative of necking and fracture. It deserves mentioning that uniform elongation for this strain rate is 47 % as indicated in Table 2. The last stage of fracture is the coalescence of voids formed within the matrix.

Experimentally this stage is the most difficult stage to investigate because unlike the void initiation and growth, which tend to progress in a stable fashion, coalescence progresses rapidly and catastrophically. A detailed study by Rogers (1966) has shown that coalescence occurs by elongation of voids and elongation of the bridges of material between voids which leads to formation of a fracture surface consisting of dimples. The onset of necking is clearly revealed in thermography by the preferential heating that occurs with the temperature being maximum in the region of highest stress concentra- tion and falling of drastically on either side of the center. This is evident in Fig. 7 as well. Thus the zone of failure becomes very prominent. It can thus be concluded that the process of necking elongation and fracture of the remaining ligaments is unambiguously revealed by thermography. The sequence of thermal images for different strain values and for one typical strain rate upto fracture substantiate this observation. The fractured specimen joined together is also placed by the side in a 1:1 scale in Fig. 8.

3.4. Effect of Interrupted Straining

It can be seen from the above experiments that tensile testing at moderate strain rates (10^{-2} s^{-1}) results in a maximum temperature rise of approximately 80 K. At higher strain rates such as in press forming of metal components, less time is available for appreciable heat exchange and thus larger temperature increases could occur. Such temperature increases could affect the mechanical properties or modify the deformation properties. It has also been shown analytically by G. Ferron (1981) that development of thermal gradients plays a detrimental part in the stability of plastic flow. Ferron (1982) extended the theoretical analysis of uninterrupted straining to the case of discontinuous straining. He predicted that the removal of thermal gradient resulting from the interruption of the test, would delay the further growth of rate gradients. The analytical predictions were compared with the results from discontinuous tension tests on AISI type 304 austenitic stainless solution treated at 1323 K and then water quenched with 2 values of cross head speed corresponding to the nominal strain rates of 1.67×10^{-4} s^{-1} and 1.67×10^{-2} s^{-1}. The conclusions of his work based on the result of the mechanical test was that when restraining is performed at $\dot{\varepsilon} = 1.67 \times 10^{-4}$ s^{-1} after initial straining at $\dot{\varepsilon} = 1.67 \times 10^{-2}$ s^{-1} and interruption at $\varepsilon_1 = 0.39$, the apparent strain at maximum load is almost the same as that attained under continuous straining at

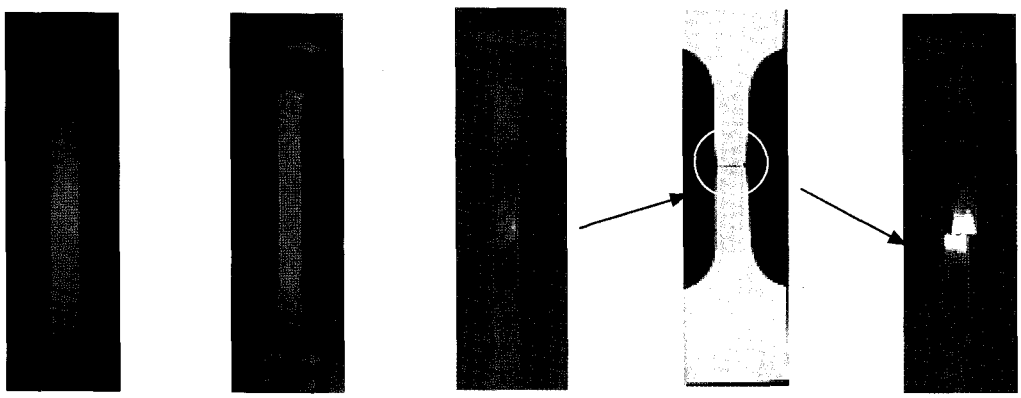

Fig. 8 Sequence of thermal images for two different strains and for a typical strain rate of 6.7×10^{-4}/sec upto fracture

$\dot{\varepsilon}$= 1.67 x 10^{-4} s^{-1}. The gain in the total elongation or the rate of change in the thermal gradient had not been investigated.

In the present experimental work, apart from investigating the effect of interruption on total elongation, an attempt has also been made to actually investigate the rate of temperature rise which is directly responsible for the alteration of mechanical /deformation properties. A set of experiments were performed, with four possible values of cross-head speed corresponding to the strain rates ($\dot{\varepsilon}$) 1.7 x 10^{-2} s^{-1}, 1.7 x 10^{-3} s^{-1}, 6.7 x 10^{-4} s^{-1} and 3.3 x 10^{-3} s^{-1}. Three typical situations were examined. In all the cases, the initial strain rate was 1.7 x 10^{-3} s^{-1} and the first stage of straining was stopped at a nominal strain of 30%. The sample was allowed to come back to room temperature and then restrained. The restraining rates in each of the cases along with the maximum temperature attained (just 2 seconds before fracture) and the total elongation is summarized in Table 4.
It can be seen from Table 4 that

(a) In the case of interrupted straining with the same strain rate being continued after interrup tion (Case A), the maximum temperature attained is lower than in case of uninterrupted straining. However the total elongation appears marginally higher only.

(b) When the strain rate after interruption is lower than the initial strain rate, the maximum temperature attained is lower and the total elongation is higher (Case B).

(c) When the strain rate after interruption is higher than the initial strain rate, the maximum temperature is also higher and the total elongation is marginally lower than in the case of uninterrupted strain rate.

Fig. 9 is a plot of variation of temperature with nominal strain in Case B. It can be observed from the slope of the curve that the rate of change of temperature is smaller after interruption as compared to the uninterrupted strain. Ferron (1981) had indicated that the interruption of strain and restraining at a lower strain rate delays the growth of temperature gradients. However, it is clearly evident from Fig. 9 and Table 4 that, when restraining is carried out at lower strain rate not only there is a delay in the growth of the temperature gradient, but the temperature rise per unit strain decreases. Consequently the maximum temperature attained at fracture decreases which results in total elongation larger than in other two cases.

Table 4 Summary of results during interrupted straining

	Initial Strain Rate (s^{-1})	Restraining Rate (s^{-1})	Temperature (K)	Total Elongation (%)
Case A	1.7 x 10^{-3}	1.7 x 10^{-3}	312	62
Case B	1.7 x 10^{-3}	6.7 x 10^{-4}	306.5	66
Case C	1.7 x 10^{-3}	1.7 x 10^{-2}	336.5	59

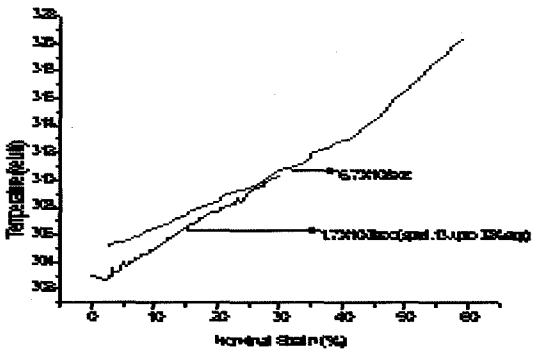

Fig. 9 Variation of nominal strain with temperature for interrupted strain rate (Case B)

4. Conclusion

The experimental results clearly indicate that thermal imaging is a valuable NDT tool that can provide detection and visualisation of transient exothermic or endothermic changes not normally observed during conventional mechanical testing.

Observations on more than 50 specimens indicate that

1. The technique can be used to identify the different stages during tensile deformation. In the elastic region, there is a small rise in temperature while the elastic to plastic transitionis characterised by a fall in temperature (thermoelastic effect) and subsequent rise. The rate of increase in tempera- ture is observed to be gradual and uniform in the work hardening zone and significant during necking. For a given nominal strain, increasing strain rate results in higher thermal emissions and higher maximum temperature attained at the time of fracture.

2. The technique provides an accurate full-field surface temperature measurements without contacting the specimen. A full-field temperature image as well as the point and time of strain localization can be easily recorded during a test. This makes it possible to visualise the region of deformation and failure. The exact point of fracture can also be predicted much in advance.

3. The effect of thermal gradients on plastic flow in case of interrupted straining has been studied. Experiments reveal that the interruption of strain and restraining at a lower strain rate not only delays the growth of the temperature gradient, but the temperature rise per unit strain decreases. Consequently the maximum temperature attained at fracture decreases which results in total elongation larger than in other two cases.

Apart from the above, such thermal measurements can provide valuable inputs to develop and validate material models that can accurately represent coupled thermal and mechanical behaviour. Thermal imaging also provides an on-line method for the detection of thermal gradients developed during extrusion and metal forming process which can be used for ensuring uniform distribution of plastic strain.

Acknowledgements

Authors are thankful to Shri S. B. Bhoje, Director, Indira Gandhi Centre for Atomic Research, Kalpakkam for his encouragement and support. The authors are also thankful to Shri P. Kalyanasundaram, Head, Division for PIE & NDT Development, IGCAR and Dr. T. Jayakumar, Head, NDT&E Section, DPEND, IGCAR for the valuable discussions.

References

Argon A. S., Im J. and Safoglu(1975), J. Cavity Formation from Inclusions in Ductile Fracture, Metallurgical Transactions, 6A, 825

Bordoni, P. G. (1986) Dislocation Micromechanics and Plastic Flow, Mechanical Properties and Behaviour of Solids, Plastic Instabilities, World Scientific Publishing Company Pvt. Ltd., Singapore, pp. 120

Caglioti, C. (1986) Thermodynamics of the Elastic Deformation and the Thermoelastic - Plastic Limit, Mechanical Properties and Behaviour of Solids, Plastic Instabilities, World Scientific Publishing Company Pvt. Ltd, Singapore, pp. 49

Chin B. A., Madsen, N. H., and Goodling J. S., (1983) Infrared Thermography for Sensing the Arc Welding Process, Welding Journal Welding Journal, Vol. 62, No. 9, pp. 227s - 234s

Dieter George, Mechanical Metallurgy, McGraw-Hill Book Company, London, 1988, pp. 434

Ferron. G, (1981) Influence of Heat Generation and Conduction on Plastic Stability under Uniaxial Tension, Material Science and Engineering, Vol. 49, pp. 241

Ferron. G, (1982) The Effect of the Interruption of Straining on Non-uniform Plastic Flow in Tension, Material Science and Engineering, Vol. 52, pp. 133-138

Gao. Y and R. H. Wagoner, A Simplified of Heat Generation during Uniaxial Tensile Test, Metallurgical Transactions A, Vol. 18A, June 1987, pp. 1001-1009

Hoffer K. O., Shaw T. W and Robertsen L. D., 93, May 1986, pp. 151-156

Huang. Y, Xu J. and Shih, C. H. Application of Infrared Technique to Research on Tensile Test, Materials Evaluation, December 1980, 76-79

Maldague P. V., Non Destructive Evaluation of Materials by Infrared Thermography, Published by Springer Verlag, London 1993, pp. 171-174

Misra A., Electromagnetic Effects at Metallic Fracture, Nature, 254, 1975, pp. 133

Raj, B. (1986) Doctoral Thesis, Acoustic Emission for Characterizing Deformation and Fracture during Tensile Testing in Austenitic Stainless Steels, Indian Institute of Science, Bangalore,

Raj, B. (1992) Venkatraman B. and C. Babu Rao, An Overview of Non-Destructive Test Application in Thermography, Journal of NDE, Sept. pp 1-13.

Raj, B. (1998) B. Venkatraman, C. K. Mukhopadhyay, T. Jayakumar, A. Lakshmi-narayana, N. Saratchandran and Ashok Kumar, Intelligent Welding Using NDE Sensors, Proc. of European Conference on NDT, Copenhagen,

Roberts C. C. Jr., (1983) Thermosense VI, Proc. of SPIE, pp. 181-187

Rockstroh T. J. and Mazumdar. J. (1985) Infrared Thermographic Temperature Measurement during Laser Heat Treatment, Applied Optics, 24, May

pp. 1343-1345

Rogers H. C., Trans. Metall. Soc. A.I.M.E. 218, 498 (1966)

Rogers L. M., (1978) Applications of Thermography in the Steel Industry, Steel Times Annual Review, 1978, pp. 661-673

Vanstone R. H., T. B. Cox, J. R. Low Jr., and J. A. Psioda, (1985) Microstructural Aspects of Fracture by Dimpled Rupture, Inter. Metal. Rev. 30, 157

Venkatraman B., Kanmani, S. C. B., Rao, D. K. Bhattacharya and Baldev Raj, Plant Condition Monitoring by Infrared Imaging, Maintenance, Vol. 12, July - Sept. 1992, pp. 27-33

Venkatraman B., Kanmani, S. C. B., Rao, Bhattacharya D. K. and Baldev Raj, B. (1993) Seventh Asian Pacific Conference on NDT, Shanghai, pp. 909 - 916

Venkataraman. B., Raj, B. Mukhopdhadyay C. K. and Jayakumar, T. (2000) Correlation of Infrared Thermographic Patterns and Acoustic Emission Signals with Tensile Deformation and Fracture Process, Review of Progress in QNDE, USA, Vol. 20, 2000, pp. 1443 - 1450

Wilburn, D. (1977) Temperature Profiles Observed in Tensile Specimens During Physical Test, Materials Evaluation, March pp. 28-31